The Flow Field of Pump Impellers with Forward and Backward Sweep

Martin Forstner, Klaus Kuhn, Wolfgang Glas, Helmut Jaberg

Institute for Hydraulic Fluidmachinery
Technical University Graz
Kopernikusgasse 24/IV
A-8010 Graz, Austria.

e-mail: Martin.Forstner@hfm.tu-graz.ac.at

Abstract

This paper presents besides traditional measurements of efficiency, head curve and cavitational behaviour, flowfield measurements within the rotating blade passage of two axial pump impellers, one with 45° forward sweep and one with 45° backward sweep, and of an unswept reference impeller. The flowfield measurements in the interblade regions were performed with a two dimensional laser Doppler velocimeter at various flow rates and with a rotating fivehole pressure probe at design flow rate.

As expected, due to the simple generation of the swept hydraulics without any compensation, head curves and efficiency of the unswept blades remain the best of all three investigated geometries. With the application of sweep the flow field changes its character from a two dimensional flow on coaxial flow surfaces into a three dimensional flow with strong interaction between the the former coaxial flow surfaces.

The results of this work shall help to improve the understanding of the effects of blade sweep on the flow field of axial impellers and shall also be a reference for fine tuning of CFD codes and comparison purposes.

1 Introduction

Sweep and dihedral of runner blades are often used on axial blowers to reduce the emission of noise. The investigation of the effects of sweep on head-curve, efficiency, cavitation and part load behaviour of axial pumps and turbines is the main aim of a continuously running research project. A design method for swept impellers, which will be able to make use of the potential of blade sweep is a far goal, which needs a detailed understanding of the effects of sweep on the three dimensional flow field within the rotating system, including the so-called secondary vortices.

There have been several studies since Smith and Yeh [1] took the two terms sweep and dihedral from aircraft engineering over into turbomachinery science. Secondary flow patterns in cascades with sweep are investigated experimentally and theoretically in [2, 3]. In [4, 5] a decrease of losses due to sweep of guide vanes for axial turbines is reported. The transport of boundary layer fluid along the surface of a swept blade was investigated in [6, 7, 8].

Skewed axial ventilators are investigated w.r.t. acoustic behaviour in [9, 10]. Skew means a

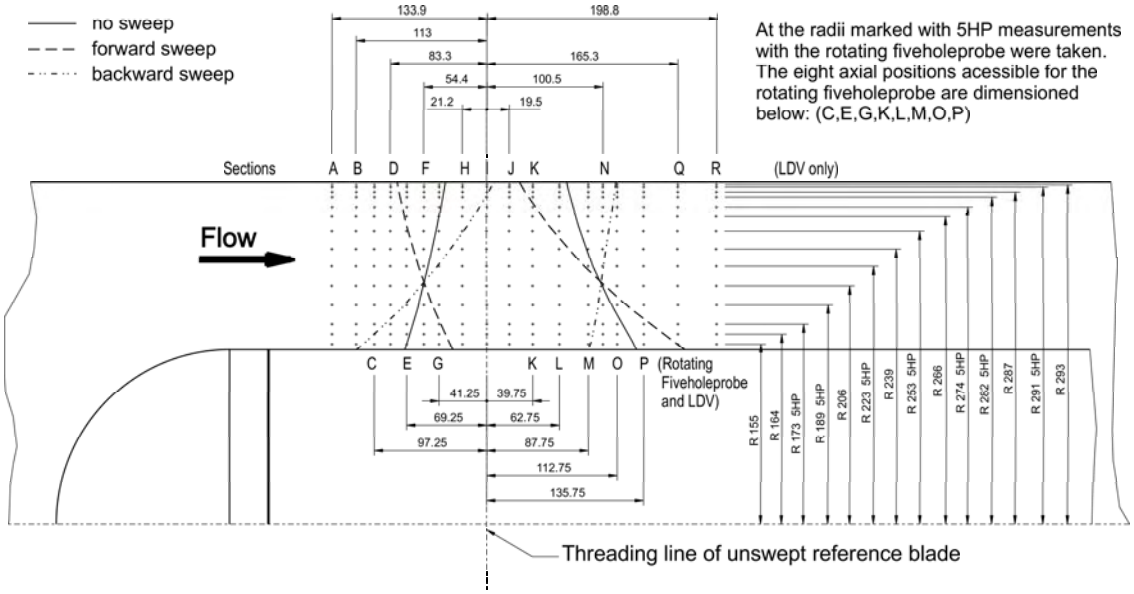

Figure 1: Grid of measurement stations at the air test rig.

shifting of blade profiles on coaxial surfaces in circumferential direction. An axial pump with high Reynolds number and backward skewed rotor blades is investigated in [11]. An overview of design methods for axial ventilators with sweep and dihedral is given in [12]. A method for calculation of the head curve of axial ventilators with skewed blades and a comparison of results with experimental data is presented in [13]. Investigations of cavitational behaviour have been reported by [14, 11, 15].

2 Experimental setup

The experimental studies have been carried out on an air test rig and a geometrically similar water test rig. The unswept blade is designed using the Lieblein [16] method (Table 1), whereas the geometries for the swept blades were found by shifting the blade profiles on coaxial surfaces against or in the direction of relative flow [17]. In this paper the direction of sweep is referred to the hub and a spanwise constant sweep angle of 45° is applied for the generation of forward and backward swept blades on both test rigs.

specific speed	n_q	210 rpm
head rise coefficient	ψ	0.298
flow coefficient	φ	0.288
hub to tip ratio	r_i/r_o	0.508
number of blades	z	5
swirl-distribution	$\psi(r)$	constant
rotational speed, water	n_{water}	1100 rpm
rotational speed, air	n_{air}	1440 rpm
radius of casing, water	$r_{o,\text{water}}$	141 mm
radius of casing, air	$r_{o,\text{air}}$	295 mm

Table 1: Design parameters of the model pump.

Both experimental setups do not include trailing guide vanes. The head and efficiency curves are measured using classical techniques. The flow field is investigated by a two dimensional laser Doppler velocimeter (LDV). The Reynolds number of the water setup is about three times higher than of the air setup, which leads to significant differences in the measured head curves and efficiencies.

At the water test rig, which is a closed loop facility, the shaft to the model pump enters through a 45° pipe bend. The casing of the model pump is made of plexi glass as optical access for LDV and cavitation observation. A detailed description of the water setup including the LDV measurement performance concerning the curved parting surface between plexiglass and water

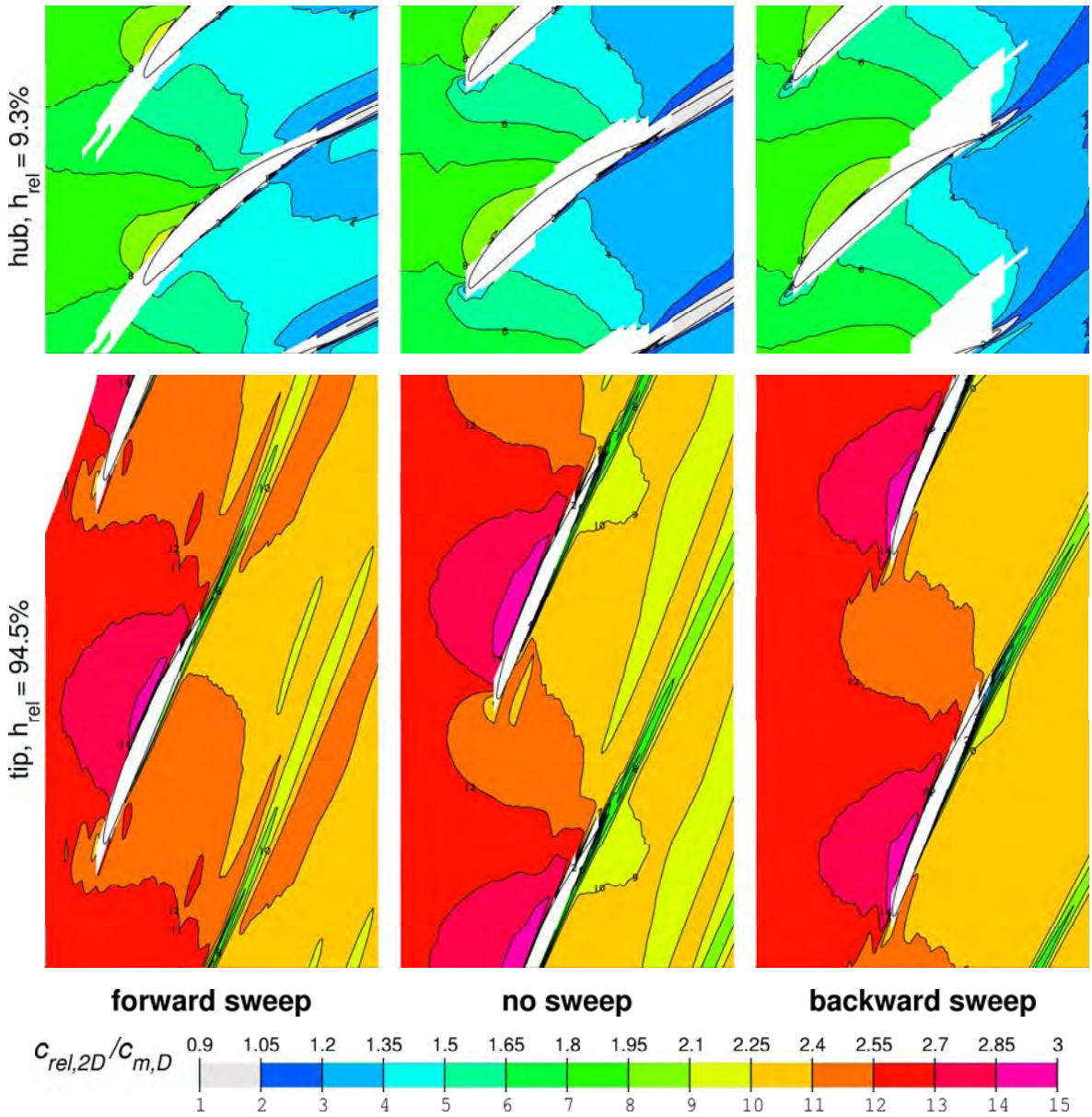

Figure 2: Relative velocity on coaxial planes, design flow rate.

is given in [17].

The open test track used for experiments in air disposes of a model hub with built-in rotating fivehole probe equipment enabling the measurement of the three dimensional velocity vector and the static pressure. The investigated blades are mounted on the model hub. In this way the hub-to-tip ratio is fixed by the geometry of the test rig. The rotating fivehole probe can be placed in eight axial positions (figure 1). For exact measurement of the hydraulic momentum a double arrangement of bearings eliminates the friction forces of the roller bearings.

Due to the runner diameter of 590 mm it is possible to use a planar parallel glass plate as optical access for LDV without changing the tip clearance conditions significantly. In contrast to the experiments in water, where the optical conditions are more complicated, coincident data can be acquired even in areas close to the hub. Figure 1 shows the grid for the flow field measurements in air.

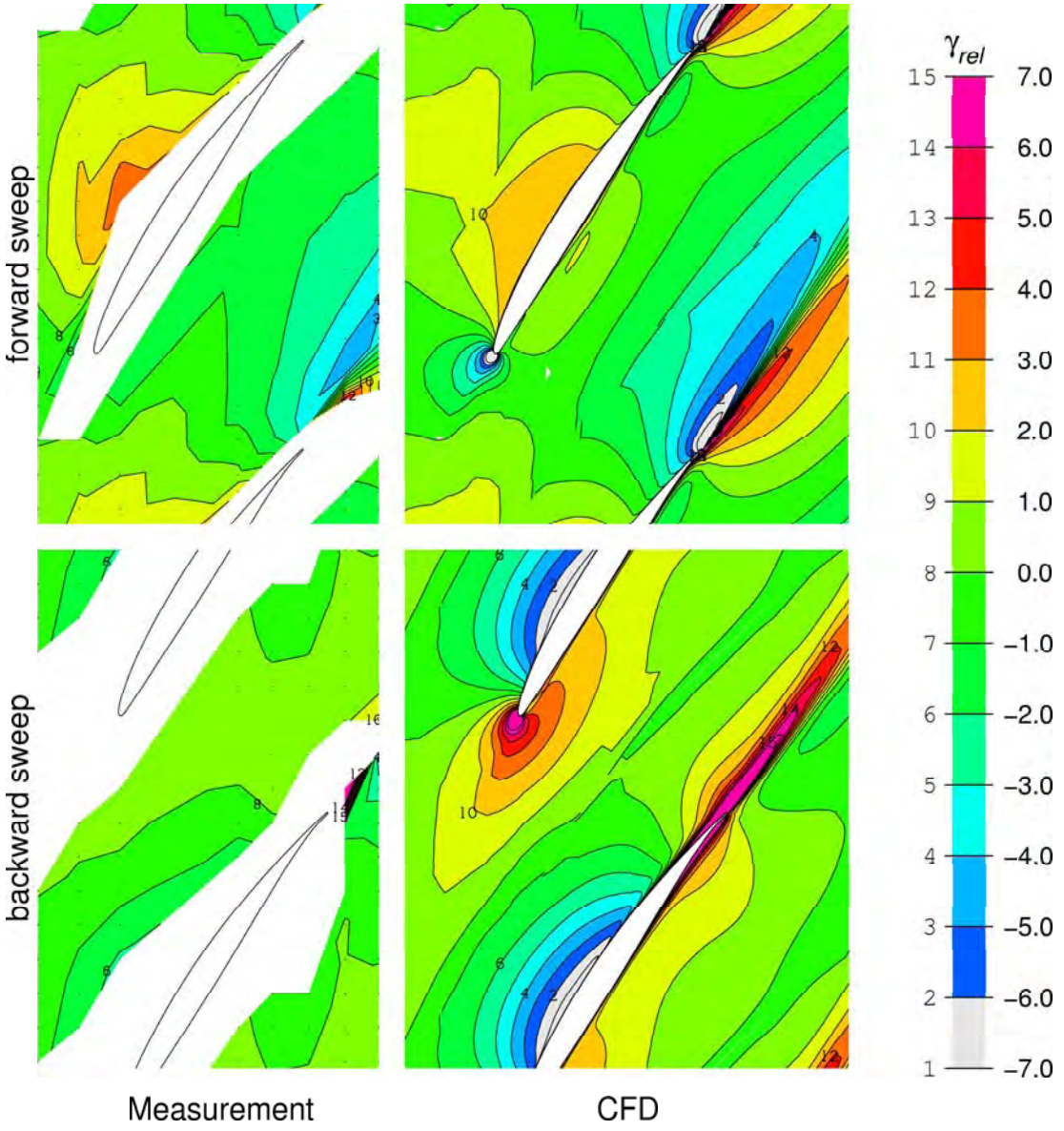

Figure 3: Flow angle γ against the coaxial surface in the middle coaxial surface, design flow rate

3 Flow field

In this section the results of the LDV flowfield measurements in air are presented. Figure 2 shows the relative velocity $c_{\mathrm{rel,2D}} = \sqrt{c_m^2 + c_u^2}$ for all investigated impellers on two coaxial surfaces, one close to the casing and one close to the hub. Here, c_m resp. c_u denote the absolute axial resp. circumferential velocity of the fluid. All velocities are made dimensionless by the mean axial velocity of the design operating point $c_{m,D}$.

At the for-running profiles (forward swept blade at casing and backward swept blade at hub) the maxima of relative velocity, which correspond to the minima of static pressure, are smaller and shifted backwards and appear approx. midcord of the suction side. This effect leads to a lower loading of these profiles and consequently to lower axial velocties after the runner in these regions, which can be observed in figure 4 showing the dimensionless axial velocity $c_m/c_{m,D}$ at normal section planes throughout the whole pump at design flow rate.

At the aft-running profiles (forward swept blade at hub and backward swept blade at cas-

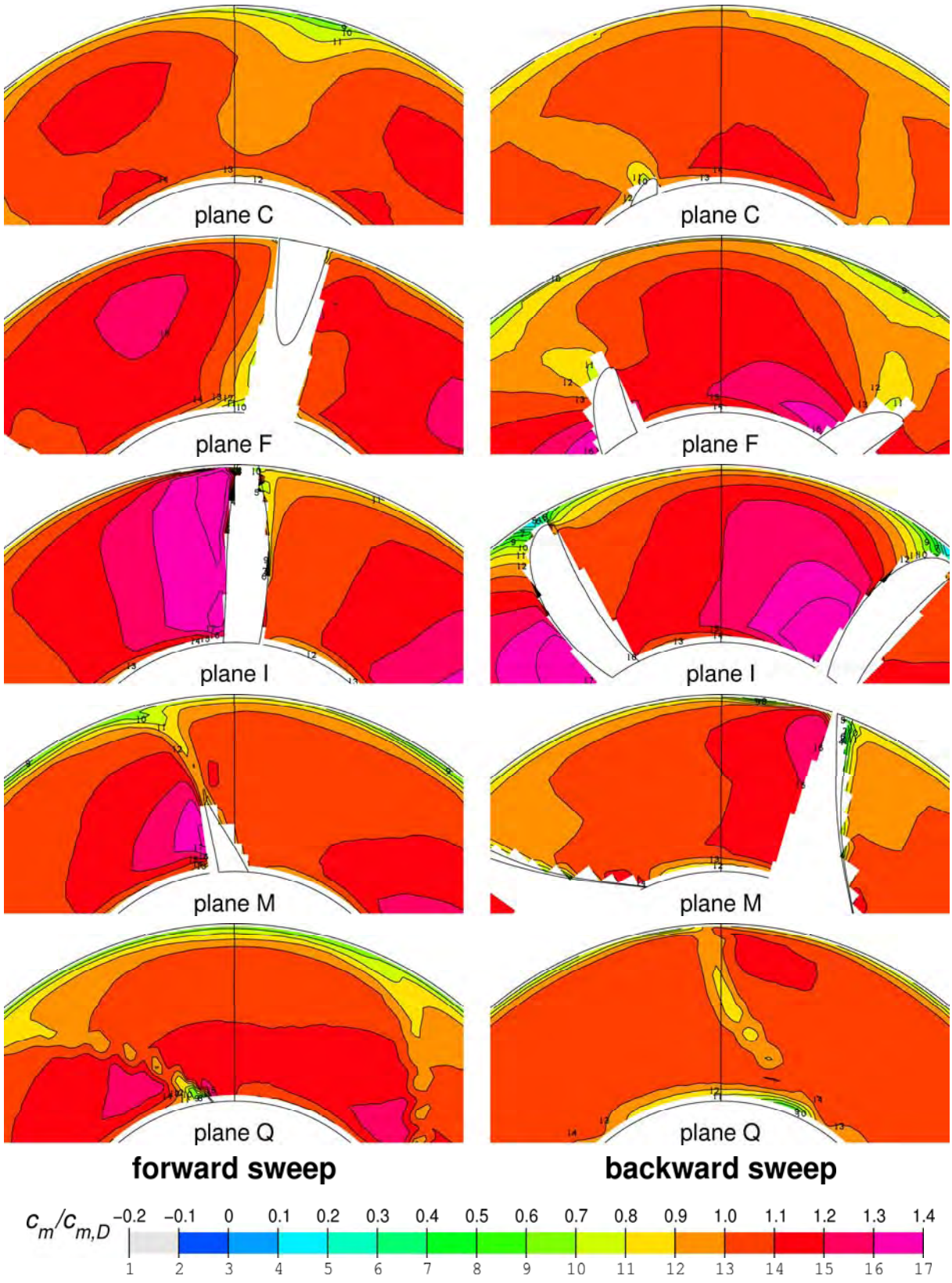

Figure 4: Axial velocity in normal sections, design flow rate, direction of rotation is clockwise, LDV measurement in air.

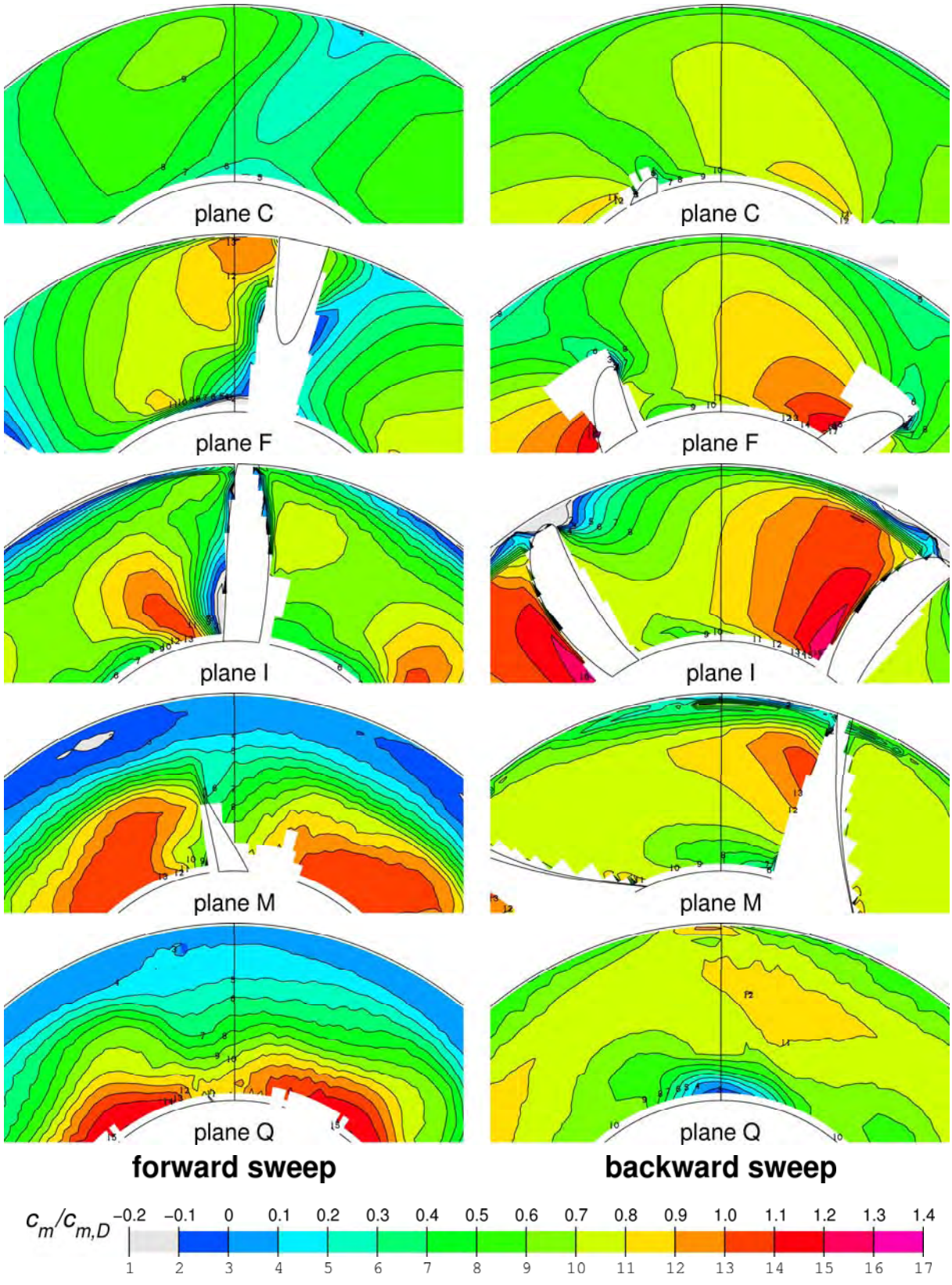

Figure 5: Axial velocity in normal sections, flow rate close to part load instabilty (forward swept runner: $Q = 0.44 \cdot Q_{\text{design}}$, backward swept runner $Q = 0.65 \cdot Q_{\text{design}}$), direction of rotation is clockwise, LDV measurement in air.

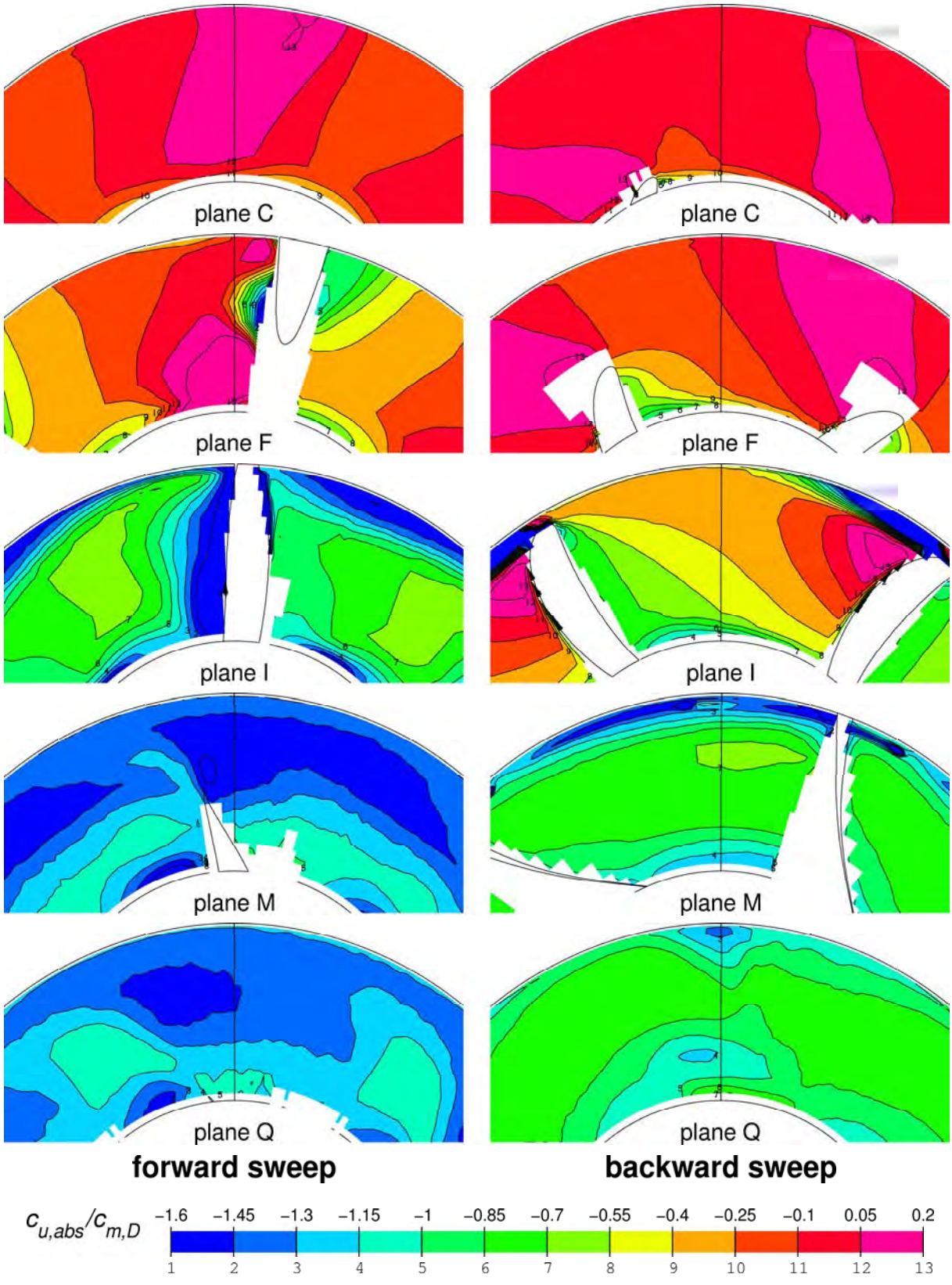

Figure 6: Circumferencial velocity in normal sections, flow rate close to part load instabilty (forward swept runner: $Q = 0.44 \cdot Q_{\text{design}}$, backward swept runner $Q = 0.65 \cdot Q_{\text{design}}$), direction of rotation is clockwise, LDV measurement in air.

ing) the influence of the neighbouring axially forward shifted profiles accelerates the flow even before the leading edge. The maxima of relative velocity are reached shortly after the leading edge. For comparison the velocity distribution of the unswept blade is also shown.

Figure 3 shows the angle $\gamma = \text{atan}(c_r/c_{\text{rel,2D}})$ resulting from the measurements with the rotating fivehole probe at midspan, where the influence of blade sweep on the radial velocity c_r is maximum. In order complete the impression of the whole interblade passage, the results pf a CFD calculation desdribed in [18] are also presented. Due to the radial pressure gradient for-running profiles attract fluid at their suction side of radii with aft-running profiles.

Figures 4 and 5 show the distribution of the dimensionless axial velocity $c_m/c_{m,D}$ measured with LDV on normal section planes throughout the whole pump at design flow rate and at an operating point close to part load instability of both swept runners. The radial movement of the flow first in the direction of the for-running profiles and at the exit in the direction of the aft-running profiles can be seen for both flow rates. At part load the forward swept runner collects the majority of the mass flow in the area of the hub, where a stable zone develops, while some recirculation can already be observed at outer radii. A similar effect at the outer radii of the backward swept runner does not develop, because of the disturbing tip leakage flow and the relative movement of the casing.

Corresponding observations can be made in figure 6 showing the dimensionless circumferential velocity $c_u/c_{m,D}$ at the operating points close to part load instability. At the suction sides of the aft-running profiles regions of stall with increased circumferential velocity is observed, whitch interacts with the tip leak flow in the case of the backward swept blade. The corresponding region of stall at the forward swept runner has only local nature which can be observed as an increased axial velocity next to the stall zone in plane I in figure 6.

Measurement uncertainities of the LDV measurements in air are approximately 1%, while the measurements of γ with the rotating fivehole probe are governed by an uncertainity of approximately 0.2°.

4 Head curves and efficiencies

The head rise of the pump is defined as the total pressure rise over the model pump. The total pressure after the pump is measured in a normal section plane approximately one chord length after the trailing edge. Due to missing trailing guide vanes it is measured on a number of radii by means of a total pressure probe and integrated with respect to the radial distribution of the mass flow.

The total pressure before the pump is calculated from the static pressure, which is measured five runner diameters upstream of the hub, and from the mean axial velocity in the measurement plane multiplied by a factor which takes the kinetic energy of the velocity profile into account.

Figure 7 shows the dimensionless head and efficiency curves for the two swept runners and the unswept reference runner measured both in water and in air. Differences in the measured pressure rise coefficient ψ of up to 0.04 result from the dependence of the losses on the Reynolds number. CFD calculations give very similar results, which are not drawn to avoid overloading of the diagrams. The same effect can be observed in the efficiency diagrams, where the optimum values differ by about 5%.

The head curves of the forward swept impellers lie about 12% below the head curve unswept reference impellers and remain stable with smaller flow rates. The head curves of the backward swept impellers lie between the head curves of the forward swept and the unswept impellers approaching the head curve of the unswept impellers for the maximal flow rates measured. The backward swept impellers stalls at the highest flow rate of all three impellers. The diagrams of

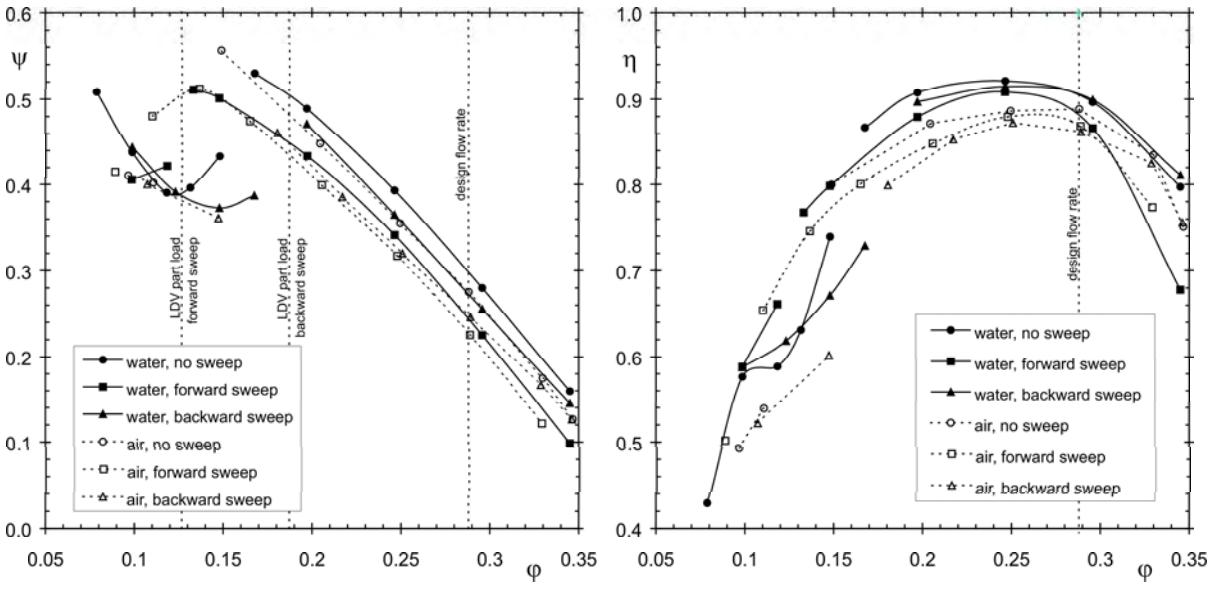

Figure 7: Head and efficiency curves.

efficiency show that, due to the simple generation of the swept hydraulics without any compensation, the unswept blades have the highest efficiency in the design area. For greater flow rates the efficiency of the backward swept runners is slightly better. Because of the better part load stability the efficiency of the forward swept blades is best for small flow rates.

Measurement uncertainties of efficiency in water are approximately 0.5%, in air approximately 1%.

5 Cavitational behaviour

As described in section flowfield the static pressure is minimum at the front part of the suction side of the aft-running profiles. The cavitation sketches (Figure 8) illustrate where the beginning cavitation occurs at NPSH of approximately 5.5 m for design flow rate and 80% part load for all three runners. Due to its relieved outer profiles, the forward swept impeller shows the best cavitational behaviour concerning the NPSH distribution over the flow rate, especially for part load.

6 Conclusions

As expected, due to the simple generation of the swept hydraulics without any compensation, head curves and efficiency of the unswept blades remain the best of all three investigated geometries. But the results presented in this paper show the basic effects of blade sweep on axial pump performance qualitatively and quantitatively. With the application of sweep in axial pump design the flow field changes its character from a two dimensional flow on coaxial flow surfaces into a three dimensional flow with strong interaction between the the former flow surfaces. The optimum distribution of the sweep angle over the radius of a pump runner with respect to efficiency, cavitational behaviour and part load stability seems to be very much dependent of the hub-to-tip ratio, the aspect ratio, the hub geometry and inlet conditions. An advanced design method which can make use of the potential of sweep, which seems to concern primarily improvement of cavitational behaviour and part load stability due to forward sweep, and optimize for the respective cases, will have to make use of CFD and optimizing algorithms [18]. The

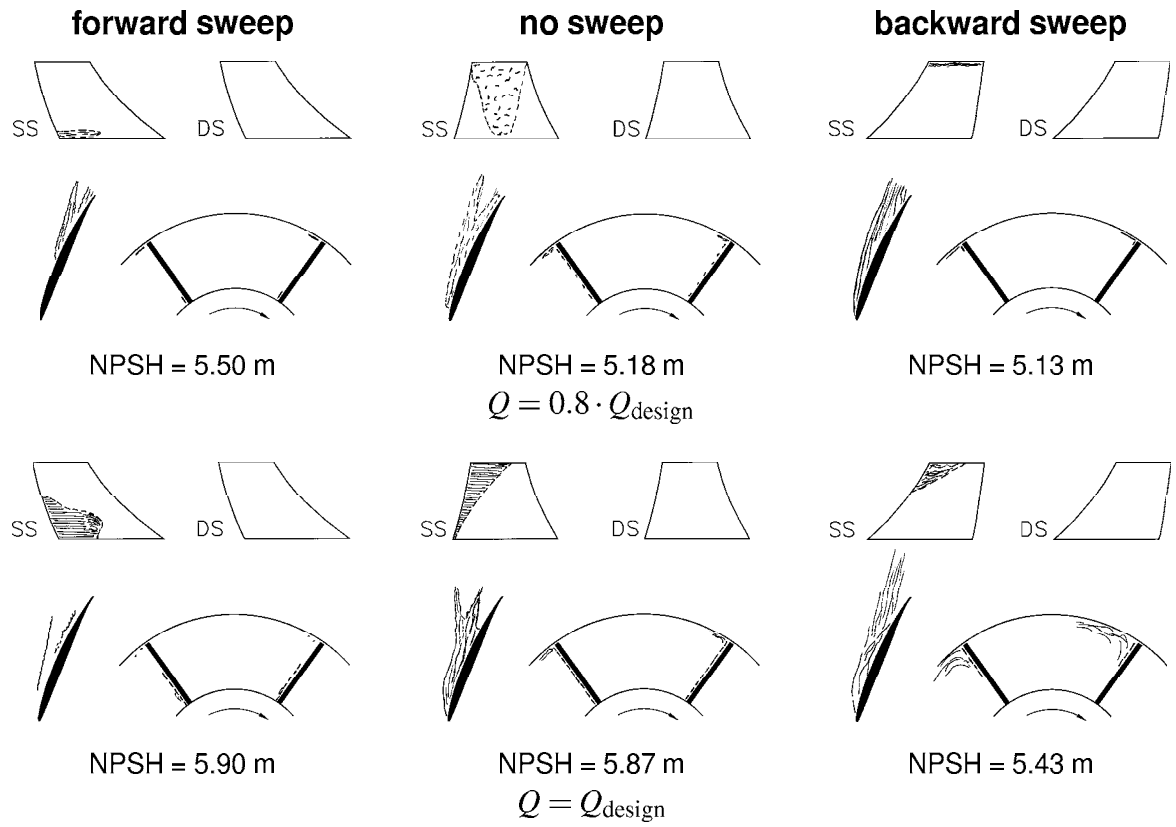

Figure 8: Cavitation sketches at design flow rate and 80% part load, four views: suction side (SS), pressure side (DS), top view and flow channel schematically.

experimental data given in this paper shall also be a reference for fine tuning of CFD codes and comparison purposes [17].

Acknowledgements

The authors would like to thank the Austrian FWF and the Jubiläumsfonds of the Austrian National Bank for supporting the research project P12072 "Swept Blades".

References

[1] Smith, L. M., Yeh, H. (1963). Sweep and Dihedral Effects in Axial-Flow Turbomachinery. *Journal of Basic Engineering*, 85, 401–416.

[2] Stark, U., Barsun, K. (1969). *Untersuchungen über den Einfluß der Machzahl und der Pfeilung auf die Sekundärverluste in Verdichtergittern bei hohen Unterschallgeschwindigkeiten*. Forschungsbericht 69-55, Deutsche Forschungs- und Versuchsanstalt für Luft– und Raumfahrt.

[3] Gotthardt, H. (1983). *Theoretische und experimentelle Untersuchung an ebenen Turbinengittern mit Pfeilung und V-Stellung*. Dissertation, TU Braunschweig.

[4] Walker, P. J. (1987). *Blade Lean in Axial Turbines: Model Turbine Measurements and Simulation by a Novel Numerical Method*. PhD thesis, Departement of Engineering, University of Cambridge.

[5] Deich, M. E., Troyanovskii, B. M., Filippov, G. A. (1990). An effective way of improving the efficiency of turbine stages. *Thermal Engineering*, 37 (10), 520 – 523.

[6] Wright, T., Simmons, W. E. (1990). Blade Sweep for Low-Speed Axial Fans. *ASME Journal of Turbomachinery*, 112, 151–158.

[7] Lichtblau, L. (1991). Aerodynamischer und akustischer Entwicklungsstand für kompakte Motorkühlsysteme. In: *VDI Berichte, Nr. 872*, 553–574.

[8] Yamaguchi, N., Tominaga, T., Hattori, S., Mitsuhashi, T. (1991). Secondary Loss Reduction by Forward-skewing of Axial Compressor Rotor Blading. In: *Proceedings of the 1991 Yokohama International Gas Turbine Congress*, II–62 – II–68.

[9] Doneit, W. (1987). *Entwicklung von Ventilatoren beliebiger Bauart mit einem integrierten computergestützten Programmsystem.* Dissertation, Universität Karlsruhe.

[10] Meixner, H. (1995). *Vergleichende LDA-Messung an ungesichelten und gesichelten Axialventilatoren.* VDI Fortschrittberichte. VDI Verlag, Düsseldorf.

[11] Zierke, W. C., Straka, W. A., Taylor, P. D. The high Reynolds Number Flow through an Axial-Flow Pump. Technical Report TR 93-12, Applied Research Laboratory – The Pennsylvania State University, November 1993.

[12] Beiler, M. G. (1996). *Untersuchung der dreidimensionalen Strömung durch Axialventilatoren mit gekrümmten Schaufeln.* VDI Fortschritt-Berichte, Reihe 7: Strömungstechnik, Nr. 298. VDI Verlag, Düsseldorf.

[13] Stark, U., Bookjans, W., Mauß, M. (1999). *Kennlinienberechnung für Axialventilatoren mit gesichelten Schaufeln.* VDI Fortschritt-Berichte, Reihe 7: Strömungstechnik, Nr. 356. VDI Verlag, Düsseldorf.

[14] Ihara, A., Watanabe, H., Shizukuishi, S. (1989). Experimental Research of the Effects of Sweep on Unsteady Hydrofoil Loadings in Cavitation. *Journal of Fluids Engineering*, 111, 263–270.

[15] Laborde, R., Chantrel, P., Mory, M. (1997). Tip Clearance and Tip Vortex Cavitation in an Axial Flow Pump. *ASME Journal of Fluids Engineering*, 119, 680–685.

[16] Lieblein, S. (1965). Experimental Flow in Two-Dimensional Cascades. In: *Aerodynamic Design of Axial-Flow Compressors* (Johnsen, I. A., Bullock, R. O., Eds.), 183–226. NASA SP-36, Washington D.C.

[17] Kuhn, K. (2000). *Experimentelle Untersuchung einer Axialpumpe und Rohrturbine mit gepfeilten Schaufeln.* Dissertation, TU Graz.

[18] Glas, W. (2000). *Optimierung gepfeilter Pumpenschaufeln mit evolutionären Algorithmen.* Dissertation, TU Graz.